Limnol. Oceanogr., 59(6), 2014, 2042–2056

doi:10.4319/lo.2014.59.6.2042

Locating *Noctiluca miliaris* in the Arabian Sea: An optical proxy approach

Patricia S. Thibodeau,[1] Collin S. Roesler,[1,*] Susan L. Drapeau,[1] S. G. Prabhu Matondkar,[2] Joaquim I. Goes,[3] and P. Jeremy Werdell[4]

[1] Bowdoin College, Brunswick, Maine
[2] National Institute of Oceanography, Dona Paula, Goa, India
[3] Lamont-Doherty, Columbia University, Palisades, New York
[4] National Aeronautics and Space Administration, Goddard Space Flight Center, Greenbelt, Maryland

Abstract

Coincident with shifting monsoon weather patterns over India, the phytoplankter *Noctiluca miliaris* has recently been observed to be dominating phytoplankton blooms in the northeastern Arabian Sea during the winter monsoons. Identifying the exact environmental and/or ecological conditions that favor this species has been hampered by the lack of concurrent environmental and biological observations on time and space scales relevant to ecologic and physiologic processes. We present a bio-optical proxy for *N. miliaris* measured on highly resolved depth scales coincident with hydrographic observations with the goal to identify conducive hydrographic conditions for the bloom. The proxy is derived from multichannel excitation chlorophyll *a* fluorescence and is validated with microscopy, pigment composition, and spectral absorption. Phytoplankton populations dominated by either diatoms or other dinoflagellates were additionally discerned. *N. miliaris* populations in full bloom were identified offshore in low-nutrient and low–N : P ratio surface waters within a narrow temperature and salinity range. These populations transitioned to high-biomass diatom-dominated coastal upwelling populations. A week later, the *N. miliaris* blooms were observed in declining phase, transitioning to very-low-biomass populations of non–*N. miliaris* dinoflagellates. There were no clear hydrographic conditions uniquely associated with the *N. miliaris* populations, although *N. miliaris* was not found in the upwelling or extremely oligotrophic waters. Taxonomic transitions were not discernible in the spatial structure of the bloom as identified by the ocean color Chl imagery, indicating that in situ observations may be necessary to resolve community structure, particularly for populations below the surface.

The Arabian Sea is one of the most productive regions in the world because of periods of strong monsoonally driven coastal upwelling and convective mixing that bring nutrient-rich waters from below the permanent thermocline to the surface waters (Wiggert et al. 2005). Monsoons act as one of the predominant climatic systems in the Arabian Sea and are generated in response to the adjacency of the large Eurasian landmass to the Arabian Sea producing intense land–sea temperature gradients. The main physical forcings that control productivity in the Arabian Sea are winter convective mixing during the northeast monsoon (NEM) in the winter, December through March, and coastal upwelling during the southwest monsoon (SWM) in summer, June through September (Parab et al. 2006). Winds associated with SWM along the northwestern coast of Africa and the Arabian Peninsula drive offshore Ekman transport and coastal upwelling in the summer and produce large coastal phytoplankton blooms (Garrison et al. 1998; Latasa and Bidigare 1998; Shalapyonok et al. 2001). The NEM produces cooling of the northern Arabian Sea in the winter, causing the surface water to sink, generating convective mixing, and injecting nutrients to the surface (Madhupratap 1999). In effect, these monsoons create two distinct blooms, a strong bloom in the summer off the coast of Somalia and a weaker bloom in the winter off the northwest coast of India and southern Pakistan (Brock et al. 1992; Banse and English 2000).

* Corresponding author: croesler@bowdoin.edu

The Arabian Sea is a relatively biodiverse ocean basin with enhanced biological activity providing large amounts of sinking particulate organic matter that maintains an extraordinarily extended deep oxygen minimum zone. The semi-enclosed basin with convergent and downwelling geostrophic circulation characteristic of subtropical gyres leads to low oxygen regeneration in the interior deep water as well as upwelling driving deep low-oxygen waters to the surface around the perimeter (Wajih et al. 2006).

Recent and significant reductions in snow coverage in the Himalayas as well as extremely high summertime landmass temperatures are implicated in driving shifts in the intensity and timing of sea-level pressure gradients from land to sea, intensifying summer monsoons, increasing productivity, and further depleting oxygen in the deep water of the Arabian Sea (Goes et al. 2005). These oxygen-depleted waters are subsequently upwelled to the surface in the northeastern Arabian Sea during the winter monsoons, and contemporaneous changes in phytoplankton composition have been observed (Parab et al. 2006; Gomes et al. 2008). The typical pattern in phytoplankton bloom succession was dominance by diatoms, followed by cyanobacteria, and then dinoflagellates with the lowest recorded concentrations (Sawant and Madhupratap 1996). However, since the 1990s the phytoplankton community has become dominated by an emergent species, *Noctiluca miliaris* (also known as the green *Noctiluca scintillans*; Parab et al. 2006; Gomes et al. 2008; S. Prakash unpubl.). Although this species has been observed extensively in the waters of

Southeast Asia, its predominance in the Arabian Sea is a recent occurrence (Harrison et al. 2011).

Combining remotely sensed seasonal bloom distribution with shipboard microscopic analysis, Gomes et al. (2008) speculate that climatic changes have led to the shift in phytoplankton composition from diatoms to dominance by dinoflagellates, specifically *N. miliaris*, in these low-oxygenated waters during the winter NEM (February–March) and the spring intermonsoon (SIM; Madhu et al. 2012). Further analysis of the satellite data (Gomes et al. 2008) reveals that the once-dominant cyanobacteria *Trichodesmium* sp. in the eastern Arabian Sea (Westberry and Siegel 2006) has been replaced by *N. miliaris* during the SIM and that the *N. miliaris* blooms are widespread not only offshore, but also in the polluted coastal waters off of India (Chaghtai and Saifullah 2006). It is thought that recent increases in coastal phosphate concentrations give *N. miliaris* a competitive advantage compared to other phytoplankton species. Observations of ammonia secretion suggest that *N. miliaris* has sufficient nitrogen for growth (Furuya et al. 2006), perhaps because of the combination of both heterotrophy and symbiosis.

N. miliaris—The phytoplankter *N. miliaris* (Fig. 1) is an unpigmented phagotrophic and omnivorous dinoflagellate that is large enough to be seen by eye (>500 μm diameter). It consumes an array of organisms including other phytoplankton, small zooplankton, fish eggs, and detritus. *N. miliaris* consumes its food using a tentacle that connects to the cytosome and can obtain food either by direct contact with food particles that land on the tentacle or by protruding mucus from the tentacle that acts as a net to catch food (Kiørboe and Titelman 1998; Chaghtai and Saifullah 2006). Although not an active vertical migrator, *N. miliaris* is highly buoyant because of its ability to secrete ammonia into the cytoplasm and maintain positive buoyancy (Furuya et al. 2006; Lirdwitayaprasit et al. 2012). Despite being relatively immobile, *N. miliaris* intercepts its food through passive migration (Kahn and Swift 1978). The high buoyancy often causes *N. miliaris* blooms to accumulate at the surface, forming noticeably discolored waters (Kiørboe and Titelman 1998).

N. miliaris is able to tolerate moderate fluctuations in both salinity and temperature, enabling it to prevail in variable hydrographic conditions (Lirdwitayaprasit et al. 2006). It is suggested that *N. miliaris* tolerates low oxygen conditions because of its symbiont, *Pedinomonas noctilucae*, photosynthesizing more efficiently than other phytoplankton in low oxygen conditions (Hansen et al. 2004; Gomes et al. 2008). This characteristic facilitates *N. miliaris* dominance during the NEM when oxygen-deficient water is upwelled (H. Gomes and J. Goes pers. comm.).

Classified as a unicellular microscopic flagellate, *P. noctilucae* belongs to the class Prasinophyceae, although it gains its green color from the pigments common to the Chlorophyceae. Both *N. miliaris* and *P. noctilucae* occur preferably at low temperatures in tropical waters (Chaghtai and Saifullah 2006). The symbiotic relationship exists because *P. noctilucae* ostensibly provides *N. miliaris* with photosynthetic products, which *N. miliaris* would not have otherwise. In exchange, *N. miliaris* gives the symbiont protection from grazing and provides the low-pH environment (4.5–5) critical to *P. noctilucae*'s survival (Furuya et al. 2006). The green pigmentation of *P. noctilucae* produces the distinctive green coloration of *N. miliaris* so different from most other dinoflagellates, specifically the absence of peridinin and the presence of chlorophyll *b* (Chl *b*).

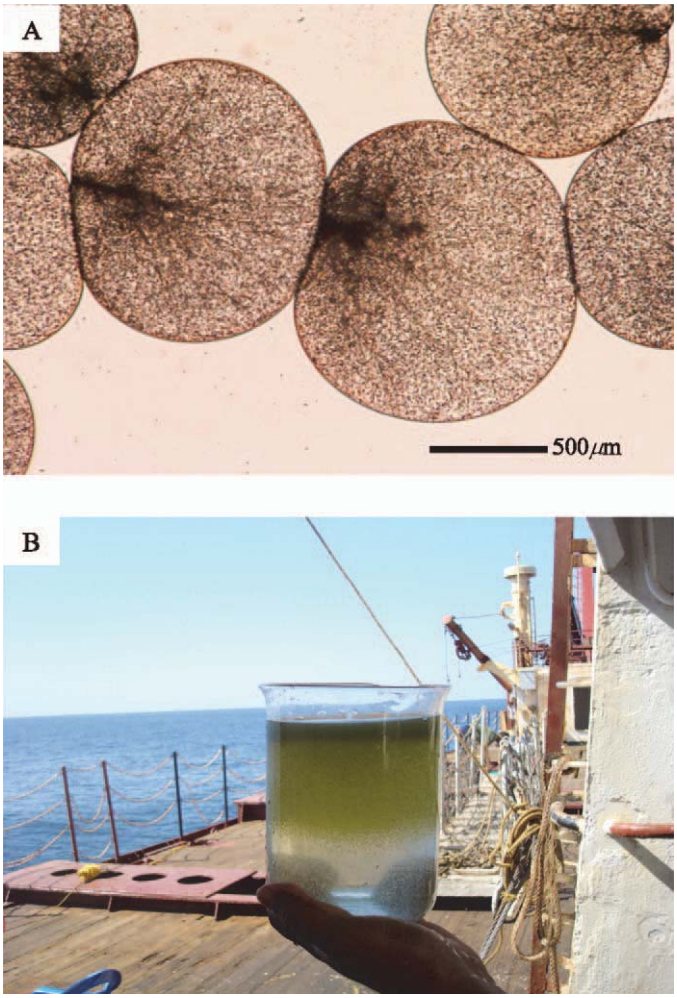

Fig. 1. (A) Microscopic image of *Noctiluca miliaris* collected from the Arabian Sea in 2009. (B) Water sample collected from the surface waters in the Arabian Sea in 2009 showing the large buoyant green *N. miliaris* cells. Photo credit J. Goes.

Taxonomic identification via pigment-based phytoplankton functional types—Although chlorophyll *a* (Chl *a*) is the primary fluorescing pigment, the energy it fluoresces originates from light absorption by the suite of accessory photosynthetic pigments (Huot and Babin 2010). Fluorescence intensity is proportional to light absorption, via the fluorescence quantum yield, and hence to pigment concentration. By using the excitation and emission characteristics associated with phytoplankton pigment fluorescence, the composition of phytoplankton communities can be determined (Yentsch and Phinney 1985; Lutz et al. 2001; Chekalyuk and Hafez 2008, 2013). Because of the distinct chlorophyte-like pigmentation, we suspected that *N.*

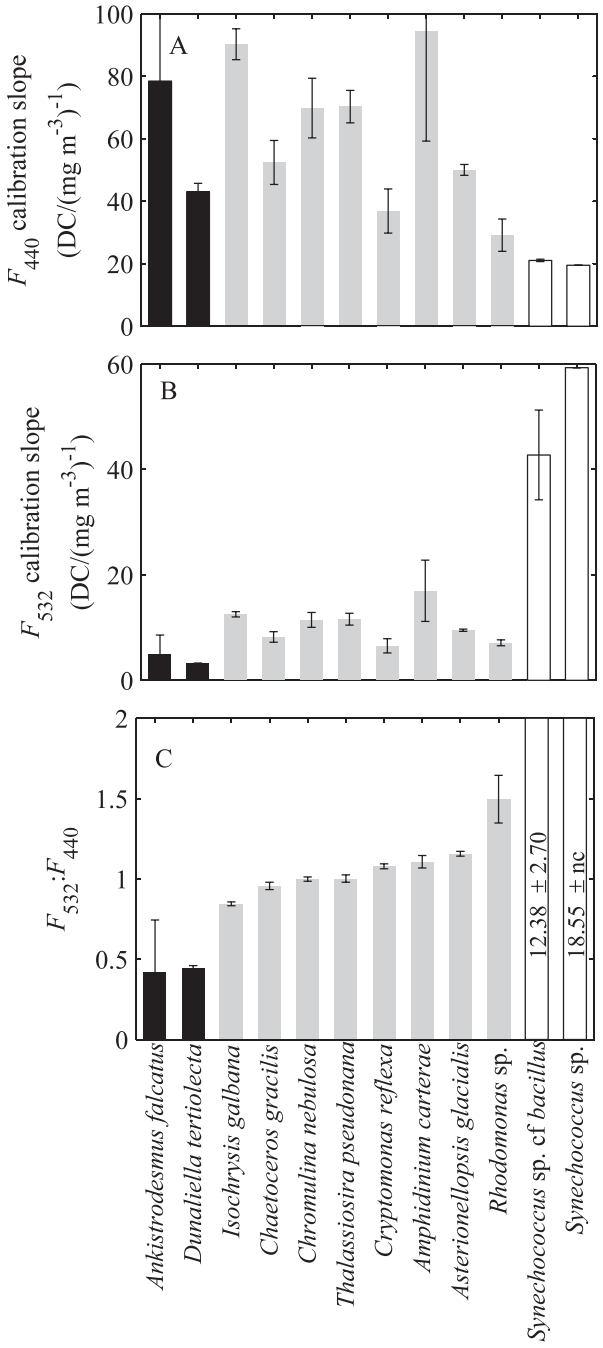

Fig. 2. Example of calibration slopes (in vivo Chl *a* fluorescence per extracted Chl *a* concentration), obtained with a WET Labs 3×1M and derived as in Fig. 3, for diverse phytoplankton species at (A) 440 nm and (B) 532 nm excitations. Error bars indicate standard deviation for cultures grown under high and low light and collected at different growth phases (data modified from Proctor and Roesler 2010). (C) Fluorescence pigment ratio (F_{532} : F_{440}) for each species after transfer function applied (*see* text). The bars for each species is shaded according to pigment lineage (black, gray, and white for green, red, and cyano lineages, respectively), following Falkowski et al. (2004) and rank ordered within lineage according to the fluorescence ratio.

miliaris would be discernible from diatoms and cyanobacteria based upon not only its pigmentation (Letelier et al. 1993; Roy et al. 2011), but its associated absorption spectra (Hoepffner and Sathyendranath 1993; Sosik and Mitchell 1995; Johnsen et al. 2011), and hence its Chl *a* fluorescence excitation (Culver and Perry 1999; Lutz et al. 2001; Richardson et al. 2010) in the blue to green range.

Proctor and Roesler (2010) calibrated the response of a multi-excitation (three-channel) Chl fluorometer to 13 different species of phytoplankton under a range of growth phases and irradiance levels. They found that the major taxonomic groups could be distinguished from each other based upon differential pigment composition. In this paper we hypothesize that the pigmentation differences between *N. miliaris* and the diatoms and cyanobacteria previously found in the northeastern Arabian Sea are sufficient to develop a robust bio-optical proxy based upon multichannel excitation of Chl fluorescence. Using this proxy, we identify the extent of *N. miliaris* populations in the northeastern Arabian Sea in situ during the winter monsoon and relate the population distribution to both the hydrographic features and the spatial structure of the satellite-derived Chl features. We further hypothesize that the distributions of *N. miliaris* will be associated with the bloom structures identified by high concentrations of satellite-derived Chl in the northeastern Arabian Sea during the winter monsoon and that these populations will occupy water masses with characteristics distinct from other phytoplankton communities. In other words, when *N. miliaris* is observed, it will be in high concentrations and will exclude other phytoplankton groups within defined water masses because of the competitive advantage that it has by both feeding on phytoplankton and receiving photosynthate from its symbionts.

Methods

Sensor calibration—The Western Environmental Technologies (WET) Labs 3×1M is a three-channel (440, 470, and 532 nm)–excitation, single-channel (695 nm)–emission detection fluorometer in their Environmental Characterization Optics Triplet sensor series. The excitation is supplied by low-power light-emitting diodes (LEDs) with full-width, half-maximum (FWHM) ranges of 24 nm for the 440 nm and 470 nm LEDs and 32 nm for the 532 nm LED. The detector optical filter has a FWHM of 70 nm and is made of RG645 Schott glass. As the sensor is a special-order system with user-defined configurations, it was not supplied with calibration factors. Proctor and Roesler (2010) quantified the response of the first sensor to a variety of phytoplankton species grown under a range of controlled growth conditions. Calibration response curves (i.e., calibration slope parameters, fluorescence : Chl, units digital counts [DC] : [mg m^{-3}]) varied 5- to 10-fold in response to pigmentation differences between species at the different wavelengths (Fig. 2A,B). The median calibration value for the 470 nm excitation (the typical excitation wavelength for most commercially available Chl fluorometers) coincided with those obtained for *Thalassiosira pseudonana*, a ubiquitous centric diatom in the red pigment

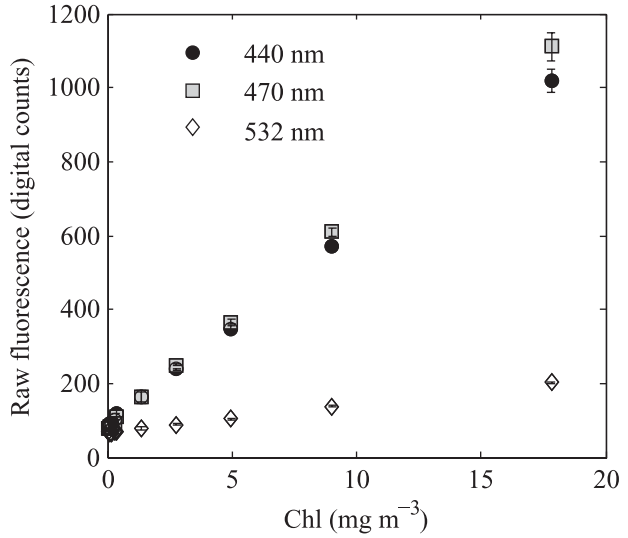

Fig. 3. Standard calibration curves for each excitation channel of the WET Labs 3×1M sensor using a dilution series of *Thalassiosira pseudonana*. The y error bars represent the standard deviation of a 60 s burst sample of raw fluorescence for each dilution, and the x error bars represent the standard deviation of triplicate extracted Chl *a* analyses for each dilution. Calibration slopes are computed from type II linear regression.

lineage. Dinoflagellates typically had higher calibration slopes and cyanobacteria and chlorophytes had lower slopes. In addition, the calibration slopes obtained for *T. pseudonana* were repeatable within 5% among calibrations separated by years as long as the growth conditions were replicated. This provides a useful means for computing a transfer function between sensors, essentially adjusting for difference in gain at each excitation wavelength. After adjustment by the transfer function, the species-specific calibration factors obtained by Proctor and Roesler (2010) can be computed for any sensor with the same optical configuration. We used this approach to recalibrate both the original sensor (serial number SN 001) and a newer sensor (SN 004), the latter of which was deployed in the Arabian Sea.

An acclimated culture of *T. pseudonana* (CCMP 1335) was grown in sterile filtered L1 medium (a vitamin-, trace metal–, and nutrient-enriched seawater; Guillard and Hargraves 1993, as modified by Guillard and Morton 2003) under controlled light conditions (12 : 12 light : dark cycle at 250 μmol photons m^{-2} s^{-1}) and harvested in exponential growth at a concentration of approximately 20 mg m^{-3} Chl *a*. A series of 10 dilutions of the culture was made, starting with 100% culture and decreasing by a factor of two via dilution with the same filtered seawater used for media. Two blanks were also run: Barnstad Nanopure® water and the filtered seawater diluent. Subsamples from each of the 10 culture dilutions were filtered for triplicate extractive Chl *a* analysis (Yentsch and Menzel 1963).

The absorption spectrum for the culture of *T. pseudonana* was determined spectrophotometrically from a subsample of the culture filtered onto a glass fiber filter (Whatman GF/F). The particulate absorption analysis was performed on the Cary 300 UltraViolet visible spectrophotometer following Kishino et al. (1985) for separation of phytoplankton and non-algal particle absorption and Roesler (1998) for configuration and absorption calculations. The absorption spectrum for *T. pseudonana* was then compared to that for previous calibrations of instrument SN 001 (Proctor and Roesler 2010) to ensure consistent absorption ratios (within 5% coefficient of variation) at the fluorometer excitation wavelengths between calibrations.

A type II regression analysis of the median fluorescence values for each wavelength at 440 nm, 470 nm, and 532 nm and the extracted Chl *a* concentrations for each dilution was performed (Fig. 3). The linear relationship is of the form $Y = M \times X + B$, where Y is the observed fluorescence (units DC), X is the concentration of the calibration component Chl (mg m^{-3}), M is the slope of the response (DC : [mg m^{-3}]), and B is the y-intercept, representing the signal from the media blank (DC). Instrumental dark values, F_{dark} (units DC), were measured with the optical face of the sensor covered in electrical tape and submerged in the media as recommended by the manufacturer. From this calibration, in situ Chl *a* concentration can be estimated from the sample fluorescence, F_{sample}, using the expression

$$\text{Chl } a \text{ (mg m}^{-3}) = (F_{\text{sample}} - F_{\text{dark}})/M_{\text{cal}} \quad (1)$$

where F_{dark} is the dark reading of the sensor at the specific wavelength and M_{cal} is the calibration slope determined for the *T. pseudonana* culture for that specific wavelength. Each time the sensor is used to quantify Chl, a media blank reading is collected using filtered sample (either from a culture or from the natural environment). The reading is processed as if it were a sample, the media-specific Chl value, which is subsequently removed from each sample value (Davis and Cullen 2003). Typically this value is not significantly different from zero; however, exceptions are found, particularly in waters with high-colored dissolved organic matter (Proctor and Roesler 2010).

Transfer functions between sensors—Just as sensors are calibrated through time to account for instrument drift, so too are multiple sensors intercalibrated with the same standards to quantify and account for differences in gains (response curves) for each excitation/emission pair. By computing the ratio of the gains for the *T. pseudonana* culture, a transfer function between the two 3×1M sensors (SN 001 and SN 004) was computed at each wavelength (T_λ^{1-2}):

$$T_\lambda^{1-2} = M_\lambda^1 / M_\lambda^2 \quad (2)$$

where M_λ^1 and M_λ^2 are the *T. pseudonana* calibration slopes, M_{cal}, for sensors 1 and 2 measured at the same excitation wavelength λ. The transfer function is then applied to measured fluorescence observations of sensor 2 at wavelength λ, $F_{\text{meas}\lambda}^2$, so that the species calibration table of Proctor and Roesler (2010) can be used to compute the corrected fluorescence for sensor 2 at wavelength λ, $F_{\text{corr}\lambda}^2$:

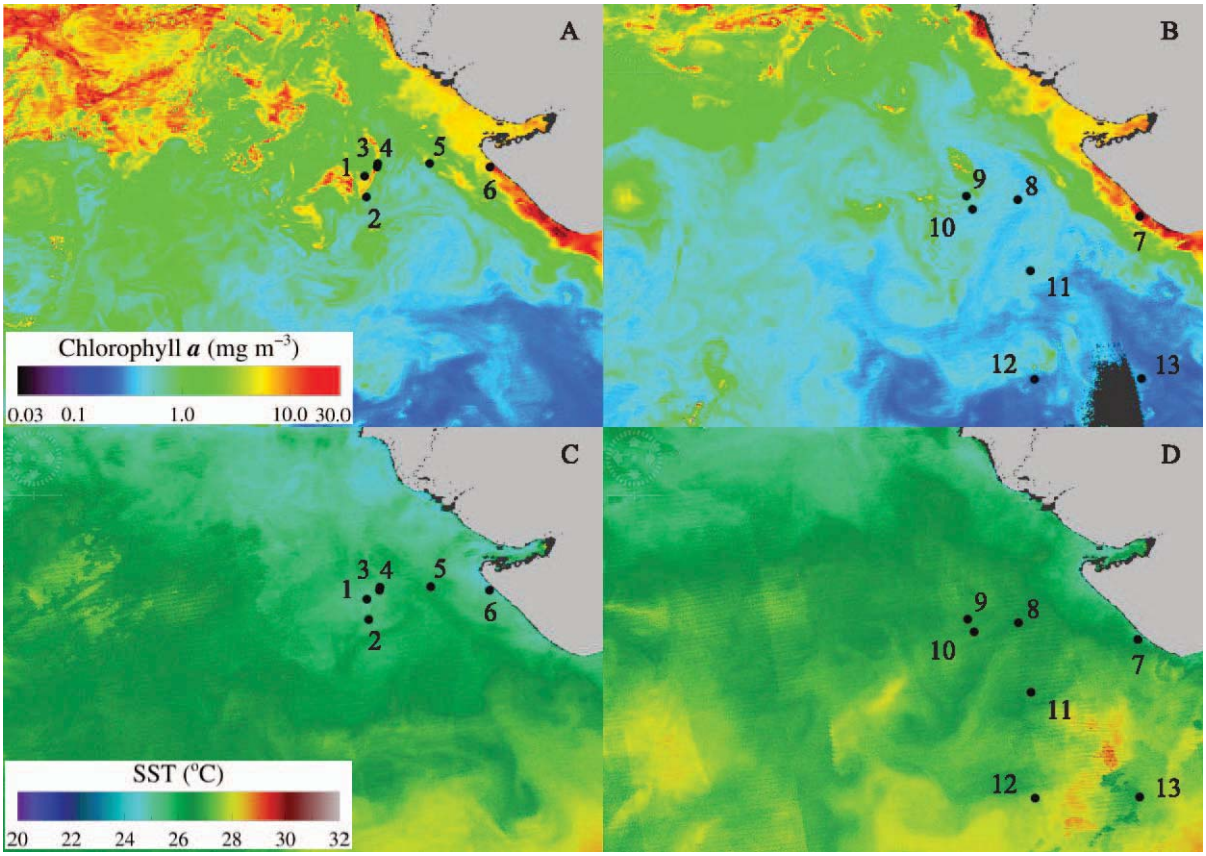

Fig. 4. Seven-day composite images of (A,B) Chl *a* and (C,D) sea surface temperature (SST) from the NASA Moderate Resolution Imaging Spectroradiometer onboard the Aqua spacecraft (MODISA). We show two temporal ranges that combine to encompass the field campaign: (A,C) 07–13 March 2011, encompassing Sta. 1 to 6, and (B,D) 13–19 March 2011, encompassing Sta. 7 to 13. We binned all data to 2 km spatial resolution. We considered all valid MODISA Chl *a* and SST retrievals when generating these composite images. Black circles indicate in situ sampling stations. Regions of gray and black indicate land and no satellite retrievals, respectively. We acquired these MODISA data from the NASA Ocean Biology Processing Group (OBPG) at Goddard Space Flight Center (http://oceancolor.gsfc.nasa.gov/cgi/browse.pl) and spatially and temporally binned the imagery using standard NASA OBPG software (http://oceancolor.gsfc.nasa.gov/seadas/).

$$F^2_{\mathrm{corr}\lambda} = F^2_{\mathrm{meas}\lambda} \times \mathrm{T}^{1-2}_{\lambda} \tag{3}$$

The transfer function serves to correct for differences between sensors and also for a single sensor between calibrations if the gains are drifting. As new species are included in the calibration table it is necessary to tie them to a calibration with *T. pseudonana* or another reference species already in the table.

Although the fluorescence response (M for each species) varies between species depending upon excitation wavelength, the fluorescence ratios are statistically different between the pigment lineages (Fig. 2C), and in some cases within lineages. The calibration slopes often do not group by lineage (Fig. 2A,B), but the ratios clearly do. The calibrated fluorescence ratio $F_{532}:F_{440}$ clearly exhibits very low values for the green lineage relative to the red lineage of the diatoms and dinoflagellates, whereas that of the cyanophyte lineage exhibits very high values compared to the red lineage. Given that the fluorescence ratios include such within-species pigment ratio variations associated with photoacclimation and growth phase (shown by error bars), we predict that the fluorescence ratios associated with *N. miliaris* will be most similar to the green lineage and therefore significantly different from the red and cyano lineages.

Field observations—In situ profiles of hydrographic and optical observations as well as water samples were collected at 13 stations aboard the R/V *Sagar Sampada* (SS286) from 06 to 21 March 2011 in the northeastern Arabian Sea (Fig. 4). At each station, fluorescence profiles were measured in concert with a Falmouth Scientific Instruments Micro conductivity, temperature, depth sensor. Discrete water samples were collected via a Niskin rosette for analyses of nutrients, pigments, absorption, and microscopy.

Nitrate, nitrite, phosphate, and silicate were determined by autoanalysis. Pigment composition was determined by high-performance liquid chromatography (HPLC) by the National Aeronautics and Space Administration's Field Support Group. Spectrophotometric absorption of particulates was measured using the quantitative filter technique (Mitchell 1990) as modified by Roesler (1998). Phytoplank-

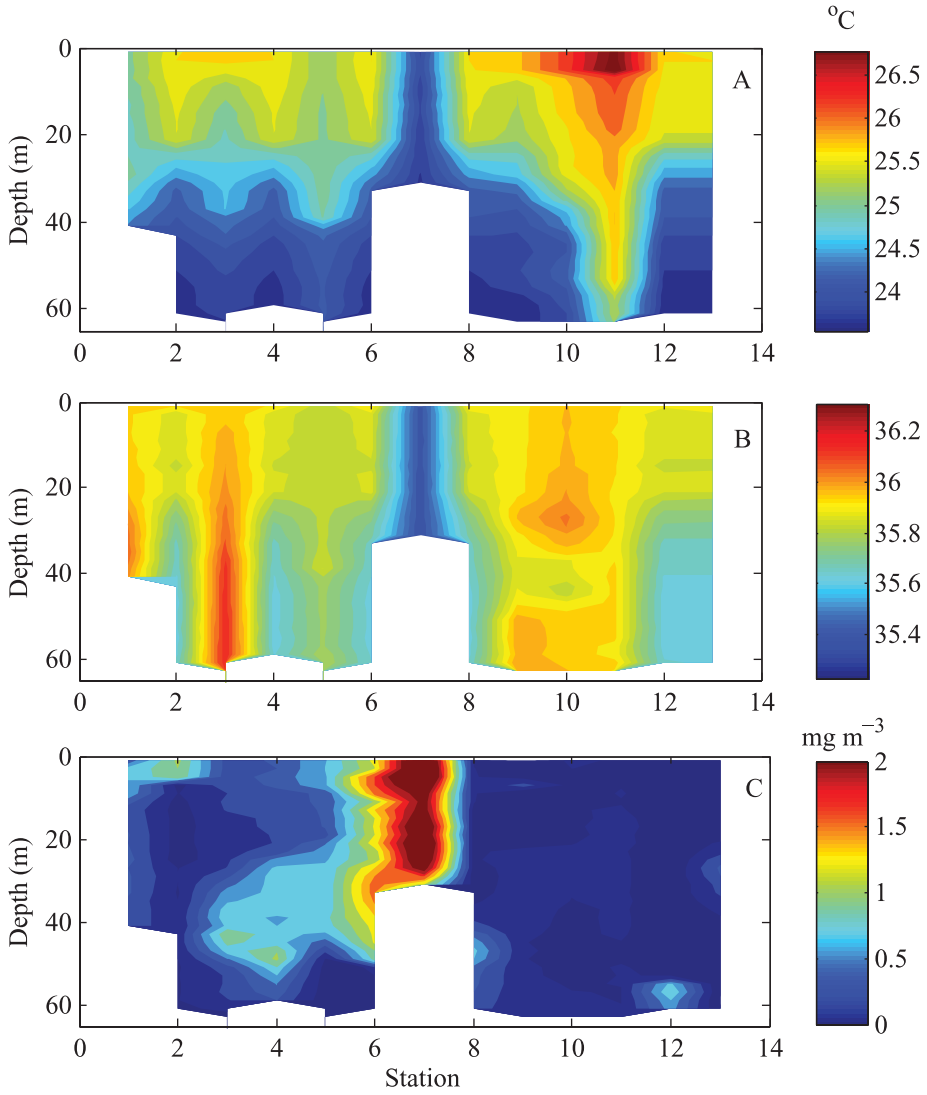

Fig. 5. Depth contour of (A) temperature, (B) salinity, and (C) Chl *a* concentration (calibrated fluorescence) measured at 13 stations along the cruise track. Maximal Chl of ~4.5 mg m^{-3} was observed at Sta. 7.

ton and non-algal fractions were determined by extraction (Kishino et al. 1985). Phytoplankton species were identified and quantified microscopically (Parab et al. 2006).

Results

The cruise began offshore in stratified waters with temperature ranging from 23.5°C to 26.8°C and salinity ranging from 35.2 to 36.3 (Fig. 5). This region appeared to be a frontal zone with stations drifting between warmer surface waters at Sta. 3 and cooler surface water at Sta. 1 and strongest thermal gradients at Stas. 2, 4, and 6. The highest salinities were observed at depth of Stas. 1 and 3 with lower salinities observed at depth of Stas. 2 and 4–6. Onshore at Sta. 7, the water was well mixed and exhibited the lowest temperature and salinity values because of strong upwelling. The return to the offshore stations showed overall surface warming with the highest temperature at Stas. 11 and 12 (Fig. 4C,D). Higher surface salinity (like Stas. 2 and 4–6) was found at Stas. 8, 12, and 13, whereas Stas. 9–11 exhibited higher salinity throughout the water column with some evidence of slightly freshened conditions at 40–50 m. Hydrographic conditions at Sta. 8 were most similar to Sta. 6, whereas Stas. 9–11 were most similar to Stas. 1, 3, and 4; Stas. 12 and 13 were hydrographically more similar to Stas. 2, 5, and 6.

An offshore surface phytoplankton bloom was observed at Stas. 1–5 (Fig. 5C), with highest concentrations at Sta. 2 and lowest at Sta.3. A subsurface population was observed at about 30–50 m at Stas. 3–5 and appeared hydrographically connected to the large coastal bloom at Stas. 6 and 7. There was a slight subsurface increase in Chl at Sta. 1 as well, but not as defined; the deep population was absent at Sta. 2. Upon return to the site of the initial surface bloom (Stas. 8–10) there was a distinct absence of the previous bloom; only a small deep population at approximately 45 m

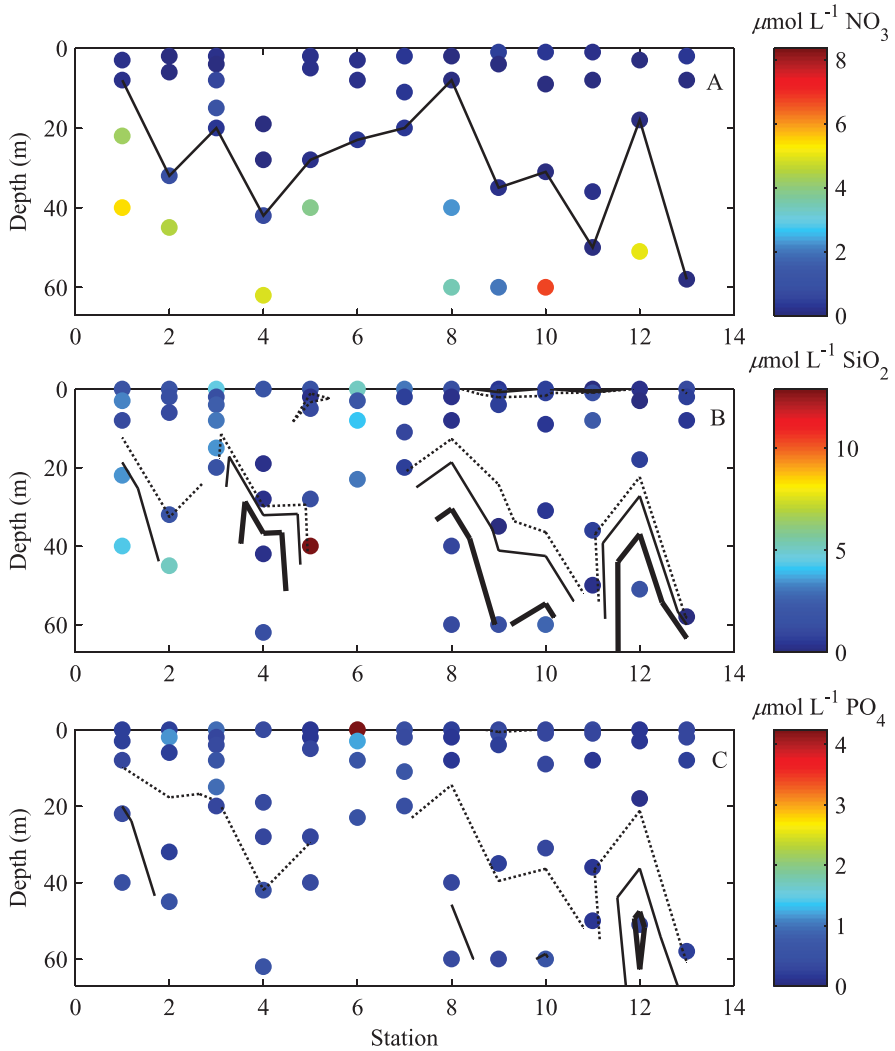

Fig. 6. Depth distribution of discrete (A) nitrate, (B) silicate, and (C) phosphate concentrations (μmol L^{-1}) measured at 13 stations along the cruise track. (A) Black line indicates the approximate top of the nitricline as determined by the maximal concentration gradient. (B,C) Contours indicate three molar ratio values of nitrate to either silicate (0.5, 1.0, and 2.0) or phosphate (1, 10, 16) concentrations; dashed, solid, and bold indicate lowest to highest molar ratio values.

at Sta. 8 was observed. The transect south evidenced two discrete populations, one at 60 m at Sta. 12 and a lower concentration at 35 m at Sta. 13. These populations were not observed at neighboring stations but were observed with two different Chl fluorometers, indicating that they were likely not artifacts.

Nutrient concentrations were generally low, with the depth of the nutricline mostly associated with the depth of the 25°C isotherm (Fig. 6). Both silicate and phosphate were generally higher in the offshore stations the first week, decreasing by week 2. The surface waters were relatively depleted in inorganic nitrogen relative to both silicate and phosphate; the latter was not observed to approach the Redfield molar ratio of 16 within the upper 60 m (Fig. 6C).

The fluorescence ratios provide insight into the phytoplankton community composition (Fig. 7). Although there is some spatial coherence between each ratio and some features in the Chl distribution, neither ratio exhibits coherence over the whole transect. The ratio of $F_{470}:F_{440}$ generally increased with depth and ranged in value from about 0.8 to 1. The ratio of $F_{532}:F_{440}$ had a much broader range, generally 0.25–0.8, although some higher values were observed in the lower biomass waters. The ratios for the near-surface Chl patch in Stas. 1 and 2 were distinct from those observed in deeper populations and were more similar to the values offshore of the coastal upwelling stations. The mid-depths of Stas. 3–5 had a population that differed significantly from the bordering population above and below it. The $F_{532}:F_{440}$ values were consistently much larger and most similar to that found at depth at Sta. 2. Discrete populations were recognizable in the small patches as observed at the bottom of Stas. 8 and 12 and at the middle depths of Sta. 13.

Distribution of phytoplankton groups—Profile fluorescence ratios in 2 m bins were plotted in ratio : ratio space

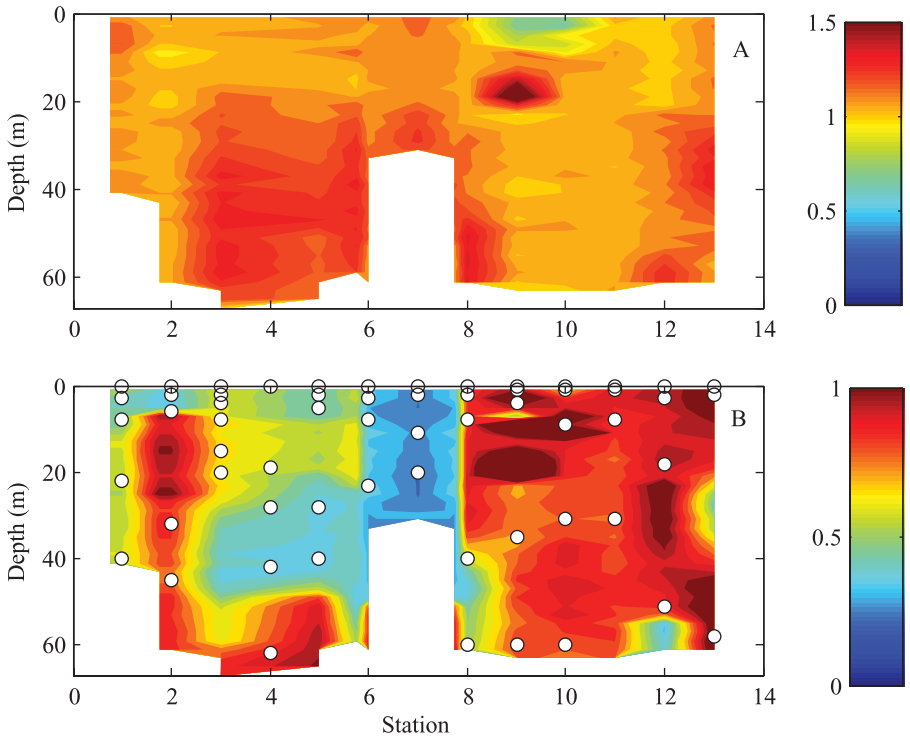

Fig. 7. Depth contour of the Chl fluorescence ratios (A) $F_{470}:F_{440}$ and (B) $F_{532}:F_{440}$. White circles indicate discrete water sampling depths used for proxy validations.

($F_{532}:F_{440}$ vs. $F_{470}:F_{440}$) to look for characteristic groupings based on taxonomic dominance (Fig. 8). Near the surface (<15 m), there were three distinct clusters of data points. The ratio values for those three clusters are consistent with those observed in laboratory cultures for diatoms and dinoflagellates in the red lineage and for the green lineage. From those three clusters of surface water observations, the values of both fluorescence ratios increase nearly monotonically as depth increases. Because both ratios have F_{440} in the denominator (essentially scaling the accessory-pigment–excited fluorescence by Chl biomass, which dominates the 440 nm signature), this pattern indicates an increase in accessory pigments relative to Chl *a* as depth increases or light decreases. This suggests that the ratios may then become proxies for photoacclimation. A cluster analysis of the fluorescence ratios and depth reveals that 89% of the variability is explained by variations in $F_{532}:F_{440}$, 8% by variations in $F_{470}:F_{440}$, and the remainder by depth variations. The three clusters of points were statistically different at $p < 0.001$, indicating that the clusters are distinct populations with respect to their paired fluorescence ratios.

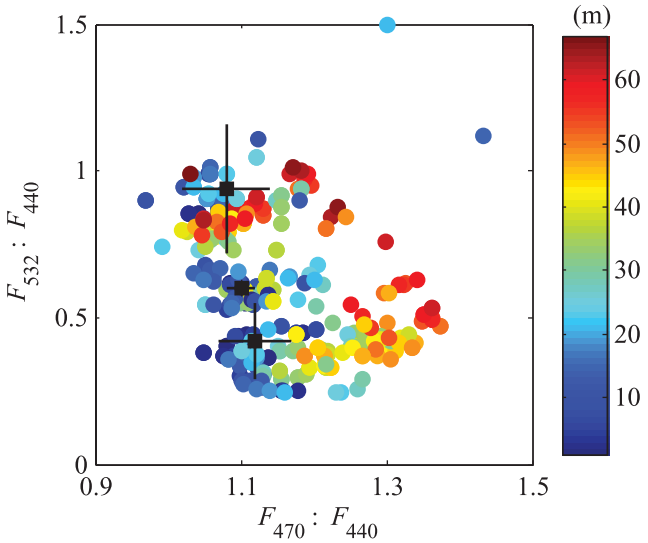

Fig. 8. Relationship between $F_{470}:F_{440}$ and $F_{532}:F_{440}$ for each 2 m depth bin along the 13 stations. Symbol color represents depth (m). The median ratios computed for discrete depths coincident with numerical dominance by each phytoplankton group are indicated by black symbols; error bars indicate standard deviations (values from Table 2).

Identification—In order to identify which populations were associated with the three clusters identified in ratio:ratio space, the ratios were examined for those discrete depths at which absorption, pigments, and microscopic evaluations were made. When *N. miliaris* represented greater than 30% of the total phytoplankton community (by number), the fluorescence ratio $F_{532}:F_{440}$ converged to a characteristic value of 0.60 ± 0.03 (Fig. 9A). Even when *N. miliaris* represented only greater than 10% of the community by number, the value was 0.56 ± 0.06. Similar results were found for diatom- and dinoflagellate-dominated communities for each ratio (Table 1). The ratios were statistically distinct between the dominant three groups and, when plotted on top of the in

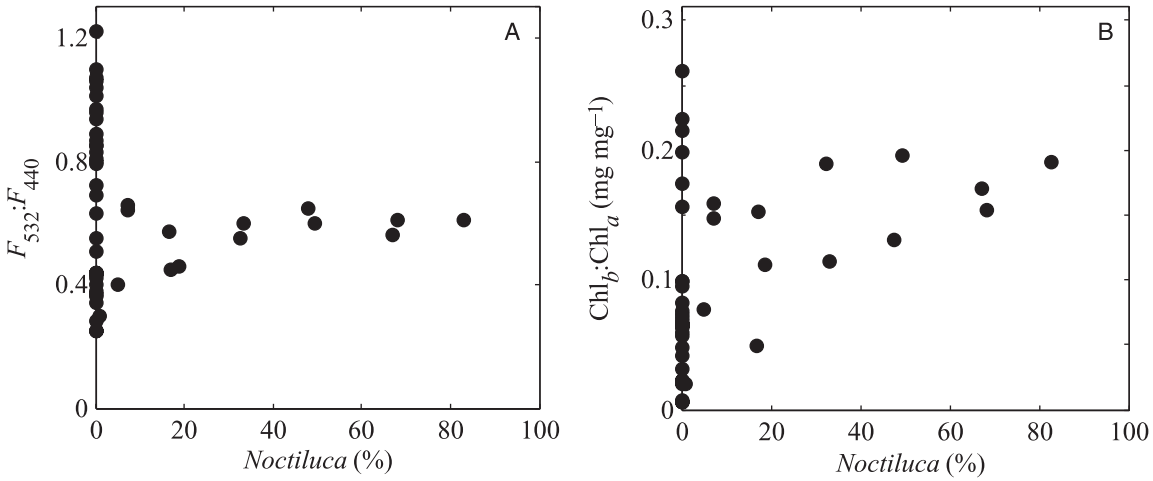

Fig. 9. (A) Chl fluorescence ratio $F_{532}:F_{440}$ and (B) HPLC-determined pigment ratio of Chl *b*:Chl *a* as a function of percentage *N. miliaris* by cell number.

situ 2 m binned observations, coincide with the three clusters (Fig. 8).

In order to link the species composition to the fluorescence ratios via pigmentation, characteristic pigmentation ratios were examined. Chl *b* in *P. noctilucae* symbionts was expected to provide the strongest pigment indicator of *N. miliaris*. A comparison between the percentage *N. miliaris* by number and the Chl *b*:Chl *a* ratio shows that there is a strong linear relationship between Chl *b* and *N. miliaris* (Fig. 9B). The Chl *b* to Chl *a* ratio observed for *N. miliaris* ranged from approximately 0.05 to 0.2 (mg Chl *b*:mg Chl *a*) and appeared as two different groupings with similar slope but different intercept values (approximately 0.08 and 0.14 [mg Chl *b*:mg Chl *a*]). These roughly correspond to surface and deep stations (i.e., high-light and low-light conditions, respectively). However, presence of *N. miliaris* alone is not sufficient to explain Chl *b* concentrations. In fact, there were seven samples with ratios above 0.15 that had no *N. miliaris*, indicating the presence of other Chl *b*–containing taxa. Interestingly, this other Chl *b*–containing community did not have the same fluorescence ratio signature as *N. miliaris* and thus would not be misidentified optically.

The discrete samples were separated according to microscopic dominance by *N. miliaris*, diatoms, and dinoflagellates and the associated phytoplankton absorption spectra distinguished by dominant group (Fig. 10). The absorption spectra cluster significantly according to microscopic evaluation, with *N. miliaris*-dominated samples exhibiting the highest blue to red absorption peak ratio and the steepest blue to green slope (e.g., 440–532 nm), followed by the dinoflagellates, then the diatoms. The systematic decrease in blue to green absorption slope is comparable to a systematic increase in green to blue absorption or accessory to Chl *a* pigment absorption. Thus the clustering observed in the fluorescence ratios is consistent with the clustering observed in absorption spectra.

Table 1. Characteristic median and standard deviation fluorescence ratios for the three major taxonomic groups observed at depths coincident with discrete samples analyzed microscopically. *Noctiluca miliaris* values computed for cases when dominance exceeded 30% by cell number (Fig. 9A). Diatom and dinoflagellate values computed for cases when dominance exceeded 60% of population and sample depths were shallower than 30 m.

Phytoplankton group	$F_{532}:F_{440}$	$F_{470}:F_{440}$
N. miliaris	0.60±0.03	1.10±0.02
Diatom	0.42±0.13	1.12±0.05
Dinoflagellate	0.94±0.22	1.08±0.06

Application—Starting with the characteristic $F_{470}:F_{440}$ and $F_{532}:F_{440}$ values determined for the samples with nearly pure community composition (Table 1) and extending those values to the depth_dependent clusters identified in ratio:ratio space (three clusters identified in Fig. 8), each 2 m bin of the in situ fluorescence profiles was assigned a dominant taxonomic group (Fig. 11). A general characterization of the stations sampled in the Arabian Sea as a function of depth and station indicated that there was an evident species shift from the beginning offshore stations to the ending offshore stations. *N. miliaris* was prevalent at the surface and mid-depths of all beginning offshore Stas. 1–5, except Sta. 2, whereas diatoms primarily characterized the deep populations of those stations (except at Stas. 1 and 2) and dominated the high-biomass coastal upwelling Stas. 6 and 7. The return to the offshore bloom (Stas. 8–10) yielded warm and salty stratified waters, quite different conditions of very low Chl concentrations, and a community dominated by dinoflagellates. The very same Chl and community characteristics were observed at Sta. 2 the week before. A remnant of the *N. miliaris* underlain by diatoms was observed below 40 m at Sta. 8.

Fluorometrically, cyanobacteria were identified in a few locations; however, some species are too small to identify microscopically for direct validation. An examination of the HPLC-derived pigment composition in those regions indicated the presence of the pigment zeaxanthin, poten-

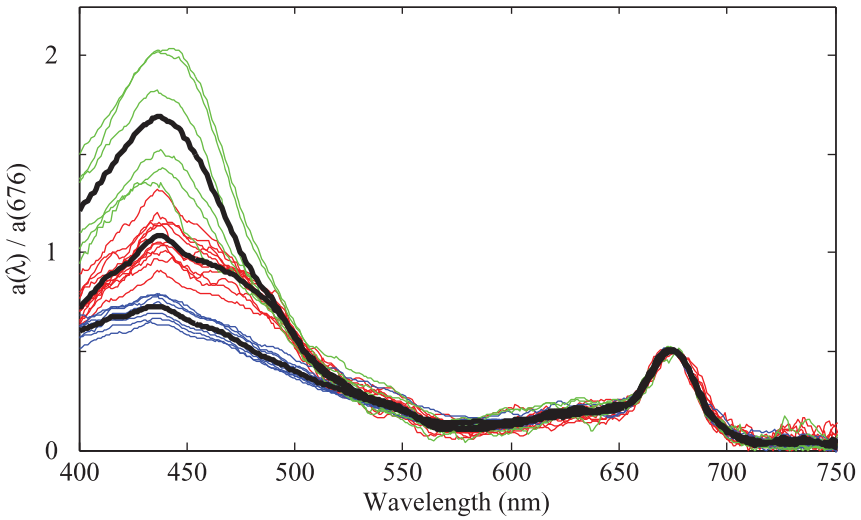

Fig. 10. Phytoplankton absorption spectra scaled to Chl *a* absorption peak at 676 nm. Spectra are color coded based upon dominance by taxonomic group determined microscopically: diatoms (blue), dinoflagellates (red), and *N. miliaris* (green). Average spectra for each group are shown in black.

tially indicating the existence of phytoplankton of the blue-green pigment class (most likely cyanobacteria) at these specific locations. However, biomass was very low in these waters, and thus the signal to noise ratio was larger. Although zeaxanthin is not unique to cyanobacteria and could therefore be indicative of other species, the high fluorescence ratios support some cyanobacterial presence.

Validation—Modeled fluorescence data were compared to measured microscopy data to confirm successful taxonomic identification at the discrete sample locations (Table 2). The fluorescence ratios falsely indicated the dominance of *N. miliaris* on two occasions; in one of those samples *N. miliaris* was a large portion of the community numerically, and, because of its large size, likely was optically dominant. In no case was a population of *N. miliaris* present and not identified by the fluorescence signatures. Fluorescence distinguished dominant taxonomic group 80% of the time, and of the 20% for which fluorescence-based dominance did not match microscopically measured dominance, it occurred either in very-low-biomass areas emitting limited fluorescence signal, or, in 7 of the 12 cases, there was a significant contribution by the group identified fluorometrically. It is notable that the diatoms are distinguishable from dinoflagellates by this approach despite somewhat similar absorption spectra, a result consistent with those of Proctor and Roesler (2010). Only eight of the discrete water samples identified *N. miliaris* microscopically, but fluorescence identified continuous populations, most of which were missed by the low-

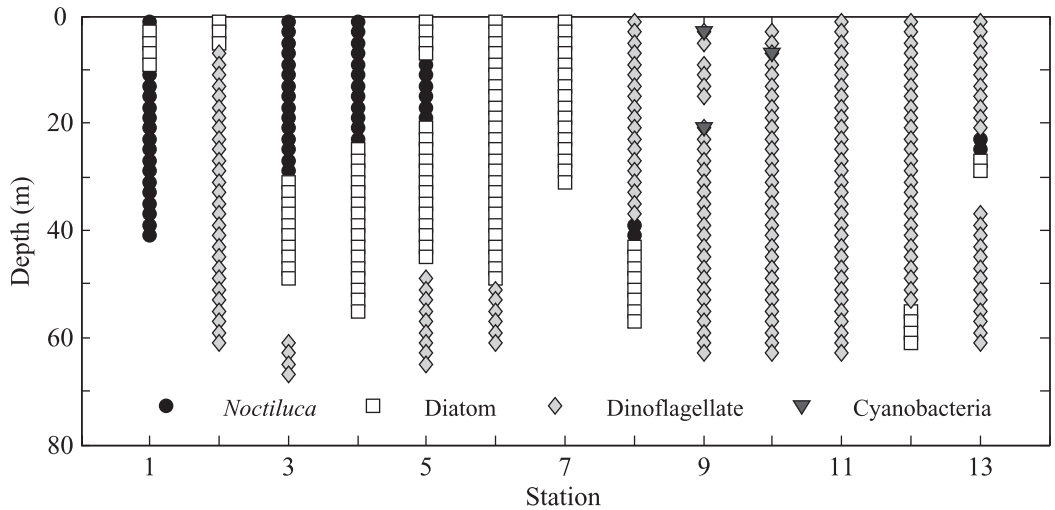

Fig. 11. Spatial distribution and dominance of *N. miliaris* and other taxonomic groups as predicted by the paired Chl fluorescence ratios. Each symbol represents a 2 m depth bin.

Table 2. Validation of modeled vs. measured taxonomic identification. Comparison between the modeled phytoplankton group estimated from the fluorescence ratio proxy and the measured phytoplankton group determined by microscopy. Numbers in bold indicate the number of groups identified that matched the modeled and measured data. Numbers in parentheses indicate number of cases for which the measured community had significant contributions by the predicted dominant group.

Modeled : measured	*N. miliaris*	Diatom	Dinoflagellate
N. miliaris	**6**	1(1)	1
Diatom	0	**27**	0
Dinoflagellate	0	10(6)	**16**

resolution water sampling, such as the deep populations at Sta. 3 and 5.

Distribution of N. miliaris—The distribution for *N. miliaris* predicted by the fluorescence ratio proxy suggests some continuous hydrographic region along Stas. 1, 3–5, which is tightly linked to distribution of diatoms in the higher biomass regions but transitions to dinoflagellates as biomass decreases. However, these features are not so clearly outlined in the satellite-derived Chl image, as Sta. 2 does not appear to be significantly different from Stas. 1 or 3 whereas Sta. 5 does appear to be a separate feature. The return track exhibits large variations in the Chl features from Sta. 8 to Sta. 13, which are lower Chl concentrations but appear to be dominated by a single group (dinoflagellates).

Hydrographically, *N. miliaris* are not uniquely found in waters of distinct temperature or salinity ranges (Fig. 12) although the observed ranges are narrower than for the other detected groups. With the exception of two data points, the temperature range is about 24.25–25.5°C and the salinity range is 35.75–36.25. But within these same temperature and salinity ranges the other three plankton groups are observed to be dominant at some locations within the cruise transect.

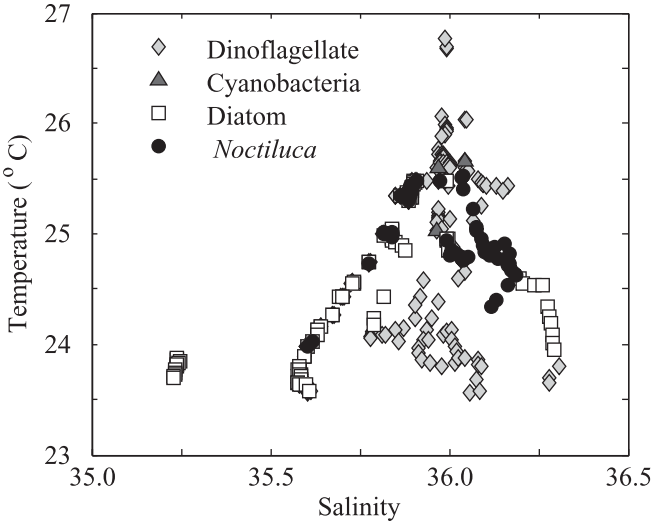

Fig. 12. Temperature–salinity diagram for the 2 m bin averaged values observed along the cruise transect. Symbols are coded by dominant phytoplankton groups as in Fig. 11.

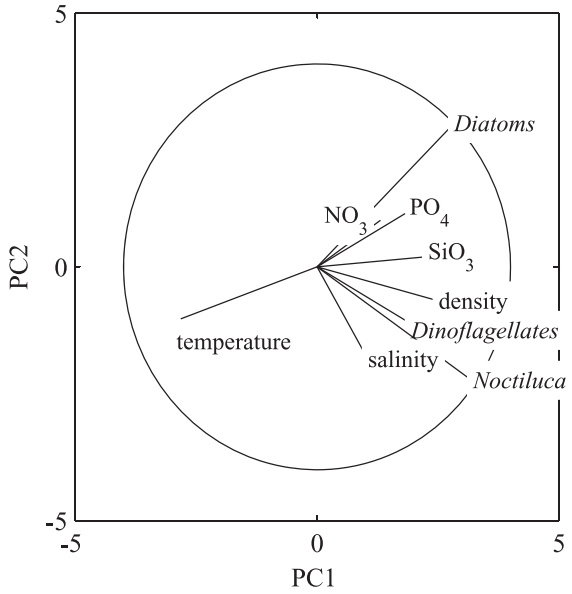

Fig. 13. Cluster analysis of discrete observations of temperature, salinity, nutrients, and log-transformed microscopic cell counts grouped into diatoms, non-*Noctiluca* dinoflagellates, and *Noctiluca*. Eighty-three percent of the variation is explained by the first two components.

A cluster analysis of the discrete observations of nutrients, hydrography (temperature and salinity), and microscopic cell concentrations of the three phytoplankton groups (log transformed) indicates that 83% of the variability in the distribution of the phytoplankton groups can be explained by two components (Fig. 13). Diatoms appear to be more covariant with colder waters that have higher nutrient concentrations, whereas *N. miliaris* and other dinoflagellates appear to covary and prefer the higher salinity waters that are characterized by low N : P ratios.

Discussion

A three-wavelength excitation Chl fluorometer, of a type that was previously calibrated to quantify the Chl-specific fluorescence response (i.e., the calibration slope) for 13 species in the laboratory (Proctor and Roesler 2010), was deployed in the Arabian Sea with the goal to develop a fluorescence-ratio–based optical proxy for the elusive dinoflagellate *N. miliaris*. Isolation of the Arabian Sea *N. miliaris* strain is challenging (S. Parab pers. comm.) and the symbiotic relationships observed in the Arabian Sea and adjacent regions are likely to vary tremendously depending upon environmental conditions (Saito et al. 2006; Sriwoon et al. 2008). Considering these constraints we used an in situ approach to develop the fluorescence ratio proxy for *N. miliaris*, statistically determining the ratio from sample depths at which it numerically dominated the phytoplankton community. Because of its exceedingly large size (and hence absorption cross section) the fluorescence proxy values were statistically significant above a numerical dominance of 10% of the total population.

A significant outcome of this analysis was the capability of using this approach to statistically distinguish diatoms

from dinoflagellates, although because of the overall smaller cell diameters and absorption cross sections, the proxy values were determined when each group was found in a higher percentage of numerical dominance. Although it has been previously demonstrated that certain species of diatoms and dinoflagellates were distinguishable under laboratory culture conditions (Proctor and Roesler 2010), extending these results to the field with mixed communities and a range of environmental conditions is encouraging. The pigment differences between the green and red lineage phytoplankton groups is significant, whereas the predominant pigmentation differences between diatoms and dinoflagellates are in their carotenoids (fucoxanthin and peridinin), which have somewhat similar absorption spectra (Roy et al. 2011).

The strength of the fluorescence ratio optical proxy approach is the capability for direct observation of the distribution of target phytoplankton species and/or pigment-based phytoplankton functional types (PFTs) measured on time and space scales consistent with hydrographic observations and on scales relevant to the ecological and physiological process of the phytoplankton. As target species and communities transition between dominance by one group over another, the continuous evolution of the proxy values from one to another provides the context for single observations. In situ validation improves confidence in the proxy signal.

The capability for discerning the depth distribution of phytoplankton groups via an optical proxy yields an approach for rapidly assessing phytoplankton populations from remote platforms such as moorings, floats, and gliders, among others, and can provide the necessary validation data sets for the next generation of ocean color sensors, such as the hyperspectral radiometer that is expected to comprise the National Aeronautics and Space Agency's Pre-Aerosol Clouds and Ocean Ecosystem mission (decadal.gsfc.nasa.gov/pace.html). Hyperspectral remote sensing promises to improve capabilities for determining pigment-based PFTs but requires depth distributions of phytoplankton populations to validate inversion algorithms (Werdell et al. 2014). Such validation data sets have been difficult to match up to satellite observations historically (Werdell and Bailey 2005) but are progressing with improved bio-optical observations and proxies for phytoplankton community structure (Werdell et al. 2013).

The continuous profiles of the fluorescence ratios in the Arabian Sea were instrumental in revealing information about the distribution and dynamics of the species *N. miliaris* with respect to the phytoplankton community. The approach allowed us to separate phytoplankton groups in situ as a function of depth. At the same time, we observed that within the range for a specific species or phytoplankton group, both fluorescence ratios increased as depth increased, consistent with the photoacclimation strategy of preferential increase in accessory pigments relative to Chl *a* as incident irradiance decreased. That the taxonomic distinctions remained separated as photoacclimation occurred indicates the robustness of the approach and the ability to use it as a means of assessing acclimation history temporally. Other environmental conditions that affect pigment composition, such as nutrient limitation and starvation (Henriksen et al. 2002), are also likely to yield variations in proxy values and by inversion provide additional physiological information under certain conditions.

Contrary to our hypotheses, the populations of *N. miliaris* were not uniquely associated with a particular water mass or water characteristics. The temperature and salinity ranges in which *N. miliaris* was found were narrower than but encompassed the ranges identified for phytoplankton communities dominated by diatoms and dinoflagellates, with the exception of the strong upwelling conditions at Sta. 7. However, it was determined that gradients in phytoplankton composition somewhat corresponded with biomass gradients—that is, as the ship moved out of the original blooms and later returned to its remnants, there was a decrease in biomass as well as a shift in the dominant phytoplankton community and as biomass decreased with depth, there was often a change in phytoplankton dominance.

The R/V *Sagar Sampada* cruise began by entering into a large *N. miliaris* bloom that was predominantly at the surface and mid-depth waters. These waters are typically oligotrophic and maximal Chl concentrations were <2 mg m^{-3}. A large bloom of diatoms appeared about 300 km from shore at a depth of 40–50 m at Stas. 3, 4, and 5 and Sta. 8 a week later. These offshore diatom populations were associated with the *N. miliaris* populations but separated by depth. This diatom population appeared contiguous with the large bloom in the upwelling along the Gujarat coast.

The exception to this pattern was observed at Sta. 2, a location that was identified at the time as the ship drifting out of the bloom. This station was characterized by very different hydrography compared to Stas. 1 and 3, and a small surface diatom population was underlain by very low Chl concentrations dominated by dinoflagellates. From satellite this station was shown to be located at the edge of the bloom, and the conditions of Sta. 2 were remarkably similar to those observed at Stas. 4, 6, and 8, albeit with much lower Chl concentrations and very different phytoplankton composition. A week later the remaining tendrils of enhanced satellite-detected Chl were associated with low concentrations of dinoflagellates and the vestige of a deep diatom population likely extending from the coastal upwelling bloom. Because the phytoplankton composition transitioned from *N. miliaris* to other dinoflagellates upon returning to the offshore stations, we suggest that the *N. miliaris* bloom had terminated by this time, allowing the prevalence of other species to occupy the water column. The presence of salps, with *N. miliaris* cells observed in their guts, confirmed that the original *N. miliaris* bloom had evolved to a demise stage.

Satellite observations confirm a declining bloom feature from the first to the second weeks of the field campaign as well as significant warming of the surface waters. However, there is nothing in the remotely sensed Chl features that would indicate the transitions in phytoplankton dominance. An analysis of these features using semi-analytical inversion of remotely sensed reflectance suggested that *N. miliaris*

populations appear on the fringes of diatom blooms (P. J. Werdell unpubl.), features that are easily missed by traditional shipboard sampling, but were captured in the continuous profiles of multichannel fluorescence. That *N. miliaris* was observed in the transition zones between well-developed diatom blooms and the low concentrations of dinoflagellate populations in the oligotrophic regions suggests a sequencing of the three groups that plays out both temporally at a single location and spatially at any given time. *N. miliaris* may be at once both grazing upon the declining diatom bloom and expanding its distribution in low N : P waters by secreting ammonia into the cytoplasm to alleviate nitrogen stress in its symbionts. Both processes are supported by the observations here.

Thus three distinct ecological regions are identified: (1) the initial *N. miliaris* bloom associated with satellite-derived Chl features, located in cooler and saltier waters to about 40 m; (2) diatom populations associated with the colder and fresher coastal upwelling features and the offshore extensions of those blooms, which are adjacent to the *N. miliaris* bloom initially and the dinoflagellate populations in later stages; and (3) the dinoflagellate-dominated community inhabiting the fringes of the satellite-derived Chl features and into the increasingly stratified, oligotrophic waters characterized by very warm and salty waters. The latter populations are found in the same salinity ranges as *N. miliaris* but in warmer temperatures. In this region the warmer temperatures are likely proxies for age of the bloom in stratified waters as temperatures of the surface increase with time. Thus, the transitions between phytoplankton communities are not necessarily associated with hydrographic features or processes such as mixing and stratification, but are indicative of the temporal evolution of species succession.

That said, there are limitations to identifying changes in *N. miliaris* dominance both through the fluorescence proxy and through satellite imagery. *N. miliaris* is no longer identifiable once it sheds its symbionts, having lost its pigments and therefore its fluorescence proxy. *N. miliaris* identification by satellite is limited to the upper depths of the water column, emphasizing the need for in situ validation such as fluorescence proxies. Although *N. miliaris* is not an active vertical migrator, its ability to secrete ammonia and maintain positive buoyancy prolongs its exposure to surface water while it is in its growth phase. Satellite imagery provides insights into phytoplankton dynamics that cannot be determined by traditional in situ sampling methods and indicates specific places and times for target species activity (Werdell et al. 2014; P. J. Werdell unpubl.). Information obtained from satellite is used in conjunction with the fluorescence proxy to understand widespread trends of *N. miliaris* distribution.

Although the oxygen data are not available, comparing the oxygen levels between the beginning and ending offshore stations would be significant in considering whether *N. miliaris* inhabits low-dissolved-oxygen waters and/or exacerbates low-oxygen zones by creating large areas of decomposition and subsequent oxygen utilization at depth during its decay. Because *N. miliaris*' supportive environment continues to widen because of increasing oxygen minimum zones as well as the expanding zone affected by agricultural runoff from the Indian subcontinent (D'Silva et al. 2012), having continuous observation of *N. miliaris* will be extremely important in the immediate and near future in order to best understand the anthropogenic and natural mechanisms supporting this species.

Contrary to our hypothesis, the populations of *N. miliaris* did not necessarily correspond with high-biomass features detected from satellite. Although the highest biomass was typically associated with the diatom population (driven largely but not exclusively by the coastal upwelling stations), the next highest biomass regions were associated with *N. miliaris* and the lowest with dinoflagellates. There was not, however, a clear demarcation in phytoplankton group dominance that corresponded exclusively to the Chl features identified in the remotely sensed imagery, suggesting that phytoplankton composition in this region did not strictly control total biomass. In other words, biomass was not a robust marker of composition as has been found for other species such as *Karenia brevis* in the waters around Florida (Stumpf et al. 2003). This implies that remote sensing approaches to detect *N. miliaris* cannot rely on biomass indicators but must incorporate spectral signatures associated with pigment absorption features and perhaps reduced backscattering efficiencies found in large, strongly absorbing phytoplankton cells (Cannizzaro et al. 2008).

Acknowledgments

Funding provided by National Aeronautics and Space Administration Ocean Biology and Biogeochemistry Program. Bowdoin College Grua and O'Connell award provided funds for travel to present this research at the 2013 Association for the Sciences of Limnology and Oceanography Conference. Special thanks to the captain and crew of the R/V *Sagar Sampada* for their dedicated efforts. P. Thibodeau wishes to thank her undergraduate honors thesis committee members, Rachel Beane and Michele LaVigne, for comments on earlier versions of the manuscript. Two anonymous reviewers provided helpful comments, for which we are very grateful.

References

Banse, K., and D. C. English. 2000. Geographical differences in seasonality of CZCS-derived phytoplankton pigment in the Arabian Sea for 1978–1986. Deep-Sea Res. II **47:** 1623–1677, doi:10.1016/S0967-0645(99)00157-5

Brock, J. C., C. R. McClain, D. M. Anderson, W. L. Prell, and W. W. Hay. 1992. Southwest monsoon circulation and environments of recent planktonic foraminifera in the Northwestern Arabian Sea. Paleoceanography **7:** 799–813, doi:10.1029/92PA01267

Cannizzaro, J. P., K. L. Carder, F. R. Chen, C. A. Heil, and G. A. Vargo. 2008. A novel technique for detection of the toxic dinoflagellate, *Karenia brevis*, in the Gulf of Mexico from remotely sensed ocean color data. Cont. Shelf Res. **28:** 137–158, doi:10.1016/j.csr.2004.04.007

Chaghtai, F., and S. M. Saifullah. 2006. On the occurrence of green *Noctiluca scintillans* blooms in coastal waters of Pakistan, North Arabian Sea. Pak. J. Bot. **38:** 893–898.

Chekalyuk, A. M., and M. A. Hafez. 2008. Advanced laser fluorometry of natural aquatic environments. Limnol. Oceanogr.: Methods **6:** 591–609, doi:10.4319/lom.2008.6.591

———, AND ———. 2013. Analysis of spectral excitation for measurements of fluorescence constituents in natural waters. Opt. Express **21:** 29255–29268, doi:10.1364/OE.21.029255

CULVER, M. E., AND M. J. PERRY. 1999. The response of photosynthetic absorption coefficients to irradiance in culture and in tidally mixed estuarine waters. Limnol. Oceanogr. **44:** 24–36, doi:10.4319/lo.1999.44.1.0024

DAVIS, R. F., AND J. J. CULLEN. 2003. The blank can make a big difference in oceanographic measurements. Limnol. Oceanogr. Bull. **12:** 29–35.

D'SILVA, M. S., A. C. ANIL, R. K. NAIK, AND P. M. D'COSTA. 2012. Algal blooms: A perspective from the coasts of India. Nat. Hazards **63:** 1225–1253, doi:10.1007/s11069-012-0190-9

FALKOWSKI, P. G., M. E. KATZ, A. H. KNOLL, A. QUIGG, J. A. RAVEN, O. SCHOFIELD, AND F. J. R. TAYLOR. 2004. The evolution of modern eukaryotic phytoplankton. Science **305:** 354–360, doi:10.1126/science.1095964

FURUYA, K., AND OTHERS. 2006. Persistent whole-bay red tide of *Noctiluca scintillans* in Manila Bay, Philippines. Coastal Mar. Sci. **30:** 74–79.

GARRISON, D. L., M. M. GOWING, AND M. P. HUGHES. 1998. Nano- and microplankton in the northern Arabian Sea during the southwest monsoon, August–September 1995 A US-JGOFS study. Deep-Sea Res. II **45:** 2269–2299, doi:10.1016/S0967-0645(98)00071-X

GOES, J. I., P. G. THOPPIL, H. D. R. GOMES, AND J. T. FASULLO. 2005. Warming of the Eurasian landmass is making the Arabian Sea more productive. Science **308:** 345–347, doi:10.1126/science.1106610

GOMES, H. D. R., S. G. P. MATONDKAR, S. G. PARAB, J. I. GOES, S. PEDNEKAR, A. R. N. AL-AZRI, AND P. G. THOPILL. 2008. Unusual blooms of green *Noctiluca miliaris* (Dinophyceae) in the Arabian Sea during the winter monsoon. Geophys. Monogr. Ser. **185:** 347–363.

GUILLARD, R. R. L., AND P. E. HARGRAVES. 1993. *Stichochrysis immobilis* is a diatom, not a chrysophyte. Phycologia **32:** 234–236, doi:10.2216/i0031-8884-32-3-234.1

———, AND S. L. MORTON. 2003. Culture methods, p. 77–97. *In* G. M. Hallegraeff, D. M. Anderson, and A. D. Cembella [eds.], Manual on harmful marine microalgae. UNESCO.

HANSEN, P. J., L. MIRANDA, AND R. AZANZA. 2004. Green *Noctiluca scintillans*: A dinoflagellate with its own greenhouse. Mar. Ecol. Prog. Ser. **275:** 79–87, doi:10.3354/meps275079

HARRISON, P. J., AND OTHERS. 2011. Geographical distribution of red and green *Noctiluca scintillans*. Chin. J. Oceanol. Limnol **29:** 807–831, doi:10.1007/s00343-011-0510-z

HENRIKSEN, P., H. K. BORIEMANN, H. M. SØRENSEN, AND H. L. SØRENSEN. 2002. Effects of nutrient-limitation and irradiance on marine phytoplankton pigments. J. Plankton Res **24:** 835–858, doi:10.1093/plankt/24.9.835

HOEPFFNER, N., AND S. SATHYENDRANATH. 1993. Determination of the major groups of phytoplankton pigments from the absorption of total particulate matter. J. Geophys. Res **98:** 22789–22803, doi:10.1029/93JC01273

HUOT, Y., AND M. BABIN. 2010. Overview of fluorescence protocols: Theory, basic concepts, and practice, p. 31–74. *In* D. Suggett, M. A. Borowitzka, and O. Prasil [eds.], Chlorophyll *a* fluorescence in aquatic science: Methods and applications. Developments in applied phycology, v. 4. Springer.

JOHNSEN, G., M. A. MOLINE, L. H. PETERSON, J. PINCKNEY, D. V. POZDNYAKOV, E. S. EGELAND, AND O. SCHOFIELD. 2011. Optical monitoring of phytoplankton bloom pigment signatures, p. 538–581. *In* S. Roy, E. K. Egeland, C. Llewellyn, and G. Johnsen [eds.], Phytoplankton pigments: Updates on characterization, chemotaxonomy and application in oceanography. Cambridge Univ. Press.

KAHN, N., AND E. SWIFT. 1978. Positive buoyancy through ionic control in the nonmotile marine dinoflagellate *Pyrocystis noctiluca* Murray ex Schuett. Limnol. Oceanogr. **23:** 649–658, doi:10.4319/lo.1978.23.4.0649

KIØRBOE, T., AND J. TITELMAN. 1998. Feeding, prey selection and prey encounter mechanisms in the heterotrophic dinoflagellate *Noctiuca scintillans*. J. Plank. Res. **20:** 1615–1636, doi:10.1093/plankt/20.8.1615

KISHINO, M., N. OKAMI, AND S. ICHIMURA. 1985. Estimation of the spectral absorption coefficients of phytoplankton in the sea. Bull. Mar. Sci. **37:** 634–642.

LATASA, M., AND R. R. BIDIGARE. 1998. A comparison of phytoplankton populations of the Arabian Sea during the spring intermonsoon and southwest monsoon of 1995 as described by HPLC-analyzed pigments. Deep-Sea Res. II **45:** 2133–2170, doi:10.1016/S0967-0645(98)00066-6

LETELIER, R. M., R. R. BIDIGARE, D. V. HEBEL, M. ONDRUSEK, C. D. WINN, AND D. M. KARL. 1993. Temporal variability of phytoplankton community structure based on pigment analysis. Limnol. Oceanogr. **38:** 1420–1437, doi:10.4319/lo.1993.38.7.1420

LIRDWITAYAPRASIT, T., P. CHUABKARNRAI, C. NITITHAMYONG, AND K. FURUYA. 2012. Effect of salinity on vertical migration of green *Noctiluca* under laboratory conditions. Coastal Mar. Sci. **35:** 70–72.

———, S. MEKSUMPUN, S. RUNGSUPA, AND K. FURUYA. 2006. Seasonal variations in cell abundance of *Noctiluca scintillans* in the coastal water off Chonburi, Province, the upper Gulf of Thailand. Coastal Mar. Sci. **30:** 80–84.

LUTZ, V. A., S. SATHYENDRANATH, E. J. H. HEAD, AND W. D. W. LI. 2001. Changes in the in vivo absorption and fluorescence excitation spectra with growth irradiance in three species of phytoplankton. J. Plankton Res. **23:** 555–569, doi:10.1093/plankt/23.6.555

MADHU, N. V., R. JYOTHIBABU, P. A. MAHESWARAN, K. A. JAYARAJ, AND C. T. ACHUTHANKUTTY. 2012. Enhanced chlorophyll *a* and primary production in the northern Arabian Sea during the spring intermonsoon due to green *Noctiluca scintillans* bloom. Mar. Biol. Res. **8:** 182–188, doi:10.1080/17451000.2011.605143

MADHUPRATAP, M. 1999. Free-living copepods of the Arabian Sea: Distributions and research perspectives. Indian J. Mar. Sci. **28:** 146–149.

MITCHELL, B. G. 1990. Algorithms for determining the absorption coefficient for aquatic particulates using the quantitative filter technique. Proc. SPIE 1302, Ocean Opt. X **1302:** 137–148, doi:10.1117/12.21440

PARAB, S. G., S. G. P. MATONDKAR, H. D. R. GOMES, AND J. I. GOES. 2006. Monsoon driven changes in phytoplankton populations in the eastern Arabian Sea as revealed by microscopy and HPLC pigment analysis. Cont. Shelf Res. **26:** 2538–2558, doi:10.1016/j.csr.2006.08.004

PROCTOR, C. W., AND C. S. ROESLER. 2010. New insights on obtaining phytoplankton concentration and composition from in situ multispectral chlorophyll fluorescence. Limnol. Oceanogr.: Methods **8:** 695–708, doi:10.4319/lom.2010.8.695

RICHARDSON, T. L., E. LAWRENZ, J. L. PINCKNEY, R. C. GUAJARDO, E. A. WALKER, H. W. PAERL, AND H. L. MACINTYRE. 2010. Spectral fluorometric characterization of phytoplankton community composition using the algae online analyzer. Water Res. **44:** 2461–2472, doi:10.1016/j.watres.2010.01.012

ROESLER, C. S. 1998. Theoretical and experimental approaches to improve the accuracy of particulate absorption coefficients from the quantitative filter technique. Limnol. Oceanogr. **43:** 1649–1660, doi:10.4319/lo.1998.43.7.1649

Roy, S., C. A. Llewellyn, E. S. Egeland, and G. Johnsen. 2011. Phytoplankton pigments: Characterization, chemotaxonomy, and applications in oceanography. Cambridge Environmental Chemistry Series.

Saito, H., K. Furuya, and T. Lirdwitayaprasit. 2006. Photoautotrophic growth of *Noctiluca scintillans* with the endosymbiont *Pedinomonas noctilucae*. Plankton Benthos Res. **1:** 97–101, doi:10.3800/pbr.1.97

Sawant, S., and M. Madhupratap. 1996. Seasonality and composition of phytoplankton in the Arabian Sea. Curr. Sci. **71:** 869–873.

Shalapyonok, A., R. J. Olson, and L. S. Shalapyonok. 2001. Arabian Sea phytoplankton during southwest and northeast monsoons 1995: Composition, size structure and biomass from individual cell properties measured by flow cytometry. Deep-Sea Res. II **48:** 1231–1261, doi:10.1016/S0967-0645(00)00137-5

Sosik, H. M., and B. G. Mitchell. 1995. Light absorption by phytoplankton, photosynthetic pigments and detritus in the California Current System. Deep-Sea Res. I **42:** 1717–1748, doi:10.1016/0967-0637(95)00081-G

Sriwoon, R., P. Pholpunthin, T. Lirdwitayaprasit, M. Kishino, and K. Furuya. 2008. Population dynamics of green *Noctiluca scintillans* (Dinophyceae) associated with the monsoon cycle in the upper Gulf of Thailand. J. Phycol **44:** 605–615, doi:10.1111/j.1529-8817.2008.00516.x

Stumpf, R. P., and others. 2003. Monitoring *Karenia brevis* blooms in the Gulf of Mexico using satellite ocean color imagery and other data. Harmful Algae **2:** 147–160, doi:10.1016/S1568-9883(02)00083-5

Wajih, S., A. Naqvi, H. Naik, D. A. Jayakumar, M. S. Shailaja, and P. V. Narvekar. 2006. Seasonal oxygen deficiency over the western continental shelf of India, p. 195–224. *In* L. N. Neretin [ed.], Past and present water column anoxia. NATO science series: IV: Earth and environmental sciences. Springer.

Werdell, P. J., and S. W. Bailey. 2005. An improved in-situ bio-optical data set for ocean color algorithm development and satellite data product validation. Remote Sens. Environ **98:** 122–140, doi:10.1016/j.rse.2005.07.001

———, C. W. Proctor, E. Boss, T. Leeuw, and M. Ouhssain. 2013. Underway sampling of marine inherent optical properties on the Tara Oceans expedition as a novel resource for ocean color satellite data product validation. Methods Oceanogr **7:** 40–51, doi:10.1016/j.mio.2013.09.001

———, C. S. Roesler, and J. I. Goes. 2014. Discrimination of phytoplankton functional groups using an ocean reflectance inversion model. Appl. Opt. **53:** 4833–4849, doi:10.1364/AO.53.004833

Westberry, T. K., and D. A. Siegel. 2006. Spatial and temporal distribution of *Trichodesmium* blooms in the world's oceans. Global Biogeochem. Cycles **20:** GB4016, doi:10.1029/2005GB002673

Wiggert, J., D. R. R. Hood, K. Banse, and J. C. Kindle. 2005. Monsoon-driven biogeochemical processes in the Arabian Sea. Prog. Oceanogr. **65:** 176–213, doi:10.1016/j.pocean.2005.03.008

Yentsch, C. S., and C. W. Menzel. 1963. A method for the determination of phytoplankton chlorophyll and phaeophytin by fluorescence. Deep-Sea Res. **10:** 221–231.

———, and D. A. Phinney. 1985. Spectral fluorescence: An ataxonomic tool for studying the structure of phytoplankton populations. J. Plankton Res. **7:** 617–632, doi:10.1093/plankt/7.5.617

Associate editor: Heidi M. Sosik

Received: 22 January 2014
Accepted: 09 July 2014
Amended: 27 August 2014